# Simulations and measurements of the transverse mode coupling instability in the LHC

D. Amorim,[1] S. A. Antipov,[1,*] N. Biancacci,[1] X. Buffat,[1] A. Mereghetti,[1,†] E. Métral,[1] N. Mounet,[1] S. Redaelli,[1] B. Salvant,[1] and D. Valuch[1,2]

[1]*CERN, Geneva, Switzerland*

[2]*Institute of Electrical Engineering, Slovak University of Technology, Bratislava, Slovakia*

(Received 3 February 2023; revised 14 November 2023; accepted 6 December 2023; published 26 December 2023)

The High Luminosity (HL) upgrade of the Large Hadron Collider (LHC) will increase the peak luminosity at the experiments by more than a factor of 5 with respect to the LHC design value. To achieve this goal, among the upgrade of several beam and machine parameters, the beam intensity will nearly double with respect to the operational LHC value, and the transverse beam emittance will decrease by 50% compared to the LHC design value. Past operational experience showed that coherent beam instabilities may occur for low, positive values of chromaticity, and a higher tune spread than predicted from simulations is required from the dedicated octupole magnets to provide enough Landau damping. With the HL-LHC brighter beams, stability margins will become tighter, and coherent instabilities become stronger if no dedicated mitigation measures are taken. An impedance reduction plan is therefore taking place targeting the collimation system, and the main contributor to the transverse beam coupling impedance at the flattop energy. New collimators with lower resistivity materials will replace the current LHC ones. In this work, we assess the benefits of this impedance reduction with respect to the transverse mode coupling instability threshold. This study quantifies the discrepancy between measured and predicted beam stability thresholds at low chromaticity. It also probes the expected gain of the impedance reduction plan of HL-LHC.

DOI: 10.1103/PhysRevAccelBeams.26.124401

## I. INTRODUCTION

Coherent beam instabilities can limit the performance reach of accelerators with high-intensity beams. For collider projects, such as HL-LHC, FCC-ee, or CEPC, this would translate into a luminosity limitation [1,2]. Instabilities have also been limitations to synchrotrons with high beam powers, such as the ISIS spallation source [3] or the J-PARC main ring [4]. Mitigation techniques, such as chromaticity, Landau damping induced by tune spread, and transverse damper are operationally used [5] to ensure machine performance.

The LHC Run 1 took place in 2010–2012 with beams of 3.5 TeV each in 2010–2011 and 4 TeV in 2012. Several coherent beam instabilities and impedance related effects occurred, limiting the reachable beam brightness. Cures were found by increasing the operational chromaticity, the tune spread through octupole magnets, and the transverse damper gain [6,7]. After the long shutdown 1 (LS1, 2013–2014) which allowed to consolidate the accelerator and increase the beam energy, the LHC Run 2 (2015–2018) took place with beams of 6.5 TeV each. A progressive reduction of the required octupole strength could be achieved during this second run. The octupoles reached a setting of 270A in 2018, while compared to 550A in 2015. This reduction resulted, among others, from a better knowledge of the control of the transverse betatronic coupling and amplitude detuning by means of linear and nonlinear optics correction. [8]. Nevertheless, a factor 2 larger octupole current is still required with respect to simulations [9]. The chromaticity could not be reduced from the operational value of $Q' = 15$ to the design value of $Q' = 2$. Another critical element needed to maintain beam stability is the transverse damper. This device consists of several strip-line beam position monitors capable of measuring the turn-by-turn transverse offset of individual bunches. Digital signal processing units then treat the bunch position data, and deflectors provide transverse kicks to each bunch. Further details on the LHC transverse damper system can be found in Ref. [10].

Dedicated measurements were performed in 2015–2017 and showed a large discrepancy between the predicted and

[*]Present address: DESY, Hambourg, Germany.

[†]Present address: CNAO, Pavia, Italy.

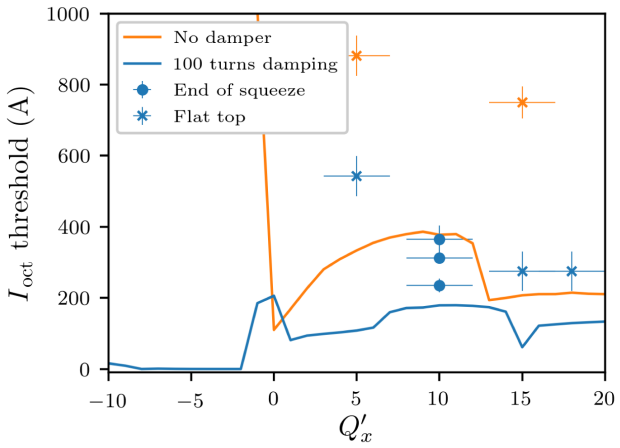


FIG. 1. Single-bunch instability threshold measurement (dots and crosses) versus predictions (solid lines) as a function of horizontal chromaticity $Q'_x$ in 2017. In orange are shown the predictions and measurements without the transverse damper while in blue are shown the case with a 100-turn transverse damper gain. Measurements are performed when the beams reach top energy (flat top, orange, and blue crosses) or at the end of the beta function reduction at the experiments (end of squeeze, orange, and blue dots). The instability threshold is shown in units of octupole current in which the beam becomes unstable. Values have been normalized to a bunch intensity of $1.0 \times 10^{11}$ protons per bunch (p.p.b.). The octupole current was reduced in steps of 20 A, waiting ~2 min at each step [11].

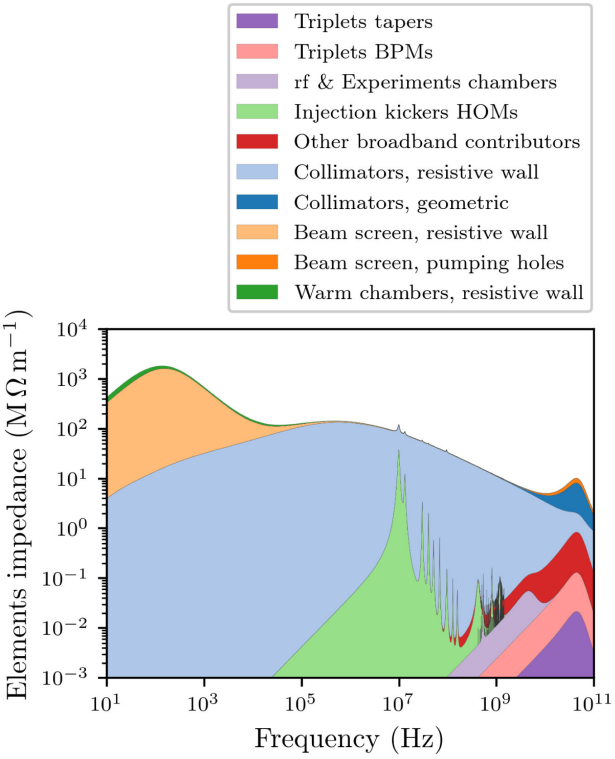


FIG. 2. Real part of the horizontal impedance model of the LHC at 6.5 TeV. Legend describes the various elements included in the model. The collimators resistive wall contribution (light blue) dominates over a large frequency range.

the measured octupole current required to stabilize the beam in the low chromaticity region. Figure 1 shows the results of single-bunch instability threshold measurements performed in 2017, highlighting the discrepancy with predictions at lower chromaticities or without the transverse damper.

The HL-LHC will use beams with a two times higher intensity ($2.3 \times 10^{11}$ protons per bunch compared to $1.2 \times 10^{11}$ protons per bunch in the LHC) compared to 2015–2018. The transverse emittances will remain similar to those achieved in 2018 (~2 μm rad), which are already 50% smaller than the LHC design values (3.75 μm rad) [12–14]. If the HL-LHC impedance remained similar to the LHC one, the machine would be more prone to transverse coherent beam instabilities.

An impedance optimization during the design phase of a project is an efficient way to reduce the risk of coherent instability. Optimizing transitions between vacuum chambers of different cross-sections, shielding cavitylike structures, and choosing low-resistivity materials are possible ways to decrease beam coupling impedance. This is for example critical for the fourth generation light sources, which make extensive use of low-aperture, nonevaporable getter-coated chambers [15] or future high-energy hadron colliders, such as FCC-hh and their collimation systems [1,16].

Figure 2 shows the real part of the horizontal dipolar impedance model of the LHC, with all elements currently included in the model. The main contributors to the LHC impedance at top energy are the collimators. The LHC collimation system [17,18] is designed to clean the beam halo and therefore protect the machine and experimental insertions. Collimators must also mitigate the consequences of regular or accidental beam losses.

Collimation systems have been used for similar purposes in other colliders, such as Tevatron [19] or SuperKEKB [20]. Next generation synchrotron light sources are also concerned about increased electron losses from the increased beam brightness. To protect insertion devices and keep a reasonable beam lifetime, collimators are also foreseen in both green field projects such as HEPS [21] and upgrades such as APS-U [22]. Such a system is already operated at the ESRF Extremely Brilliant Source [23].

In the LHC, the collimation system is composed of a hierarchy of primary (TCP), secondary (TCS), and tertiary (TCT) collimators. Figure 3 shows the collimators location along the LHC circumference. Most of them are installed in the interaction region (IR) 7 dedicated to betatron cleaning (e.g., removing particles with large transverse amplitudes and intercepting unstable bunches) and in the IR3 dedicated to off-momentum particle cleaning. Other collimator families, such as TDI and TCDQ, for injection and beam dump protection, or TCL for particle absorption around the experiments are also included in the LHC impedance model.

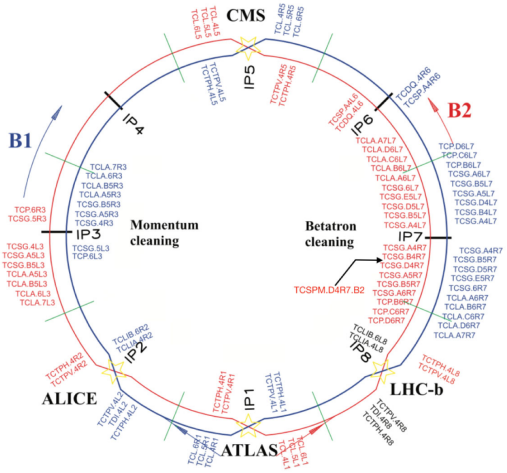


FIG. 3. Schematic representation of the LHC collimation system during Run 2 (2015–2018).

Because of the protection constraints, the collimators have gaps in the order of a few mm at top energy of 6.5 TeV, which manifests in their large contribution to the transverse beam coupling impedance. The LHC primary and secondary collimators feature jaws made of carbon-fiber-composite (CFC). Carbon-based materials present the required mechanical properties to withstand high-energy proton losses but have lower electrical conductivity compared to metallic materials.

For the HL-LHC project, an impedance reduction is taking place by upgrading several collimators using lower impedance jaw materials. Several CFC collimator have been replaced with new, low-impedance collimators during the LHC long shutdown 2 (LS2, 2019–2021) and the upgrade will be completed during long shutdown 3 (LS3, 2026–2028). The replaced collimators are those providing the largest contribution to the machine transverse impedance. An intense research and development program led to the selection of molybdenum carbide-graphite (MoGr) composites for the new collimators to be installed [24,25]. They both feature higher electrical conductivity compared to CFC while retaining the necessary mechanical strength to withstand the impact of direct or indirect beam losses. MoGr has been selected for the collimator jaws substrate and a molybdenum surface coating (Mo) can be applied to further increase the electrical conductivity. Their properties were thoroughly measured in the laboratory and with beam-based measurements, proving the resistivity reduction with respect to CFC [26,27].

In Sec. II A, we will highlight the main characteristics of the current LHC collimation system and detail the upgrade scenarios planned for HL-LHC (materials chosen for the impedance reduction and collimators targeted for the upgrade). Impedance models are computed for these different scenarios.

In Sec. II B, we use these impedance models to simulate the corresponding impact on the tune shift versus intensity and transverse mode coupling instability (TMCI) threshold. These simulation studies are used to prepare beam-based measurements performed in the LHC. Further effects that can impact the beam properties in the machine were also investigated to better prepare the measurement. The impact of chromaticity and transverse damper were checked through simulations to assess their potential impact on a tune shift measurement.

In Sec. III A, we will present the measurement and machine setup used during the dedicated measurement session in the LHC.

Section III B will detail the results of the tune shift versus intensity measurement and from these measurements the TMCI thresholds for various impedance scenarios will be estimated. Additional impedance and tune shift simulations were performed, using the machine parameters as they were during the measurement session. The tune shift measurements are compared to these additional simulations, which will also allow to estimate the discrepancy between the LHC impedance model and measurement results.

## II. SIMULATION STUDY OF THE IMPACT OF THE LHC COLLIMATION SYSTEM ON THE IMPEDANCE AND TMCI THRESHOLD

We will first describe the LHC collimation system, its working principle, and the different HL-LHC upgrade scenarios in Sec. II A. An impedance model is simulated for each scenario and is then used to predict the tune shift versus intensity and the TMCI threshold, as described in Sec. II B.

### A. LHC and HL-LHC collimation system upgrade scenarios

Each LHC ring comprises 3 TCPs and 11 TCSGs in the IR7 betatron cleaning region, all with CFC jaws. The collimator upgrade for HL-LHC will be implemented in two stages [28,29]. During LS2, for each LHC ring, two TCPs were replaced by new collimators with MoGr jaws and four TCSGs by MoGr jaws with a 5 μm Mo layer coating. The collimators selected for replacement are all located in IR7. The post-LS2 situation is the first HL-LHC impedance scenario considered. During LS3, five more TCSGs per beam in IR7 will be replaced with Mo-coated MoGr jaws. An ultimate case in which the last two TCSGs are also replaced after LS3 is the second situation considered in our simulations. This scenario was the baseline collimation upgrade until 2019. It was deemed acceptable for transverse beam stability to keep two TCSGs in CFC after the LS3 [30], hence to have 5 collimators/beam replaced during LS3 instead of 7.

We considered also the case in which the secondary collimators have MoGr jaws without coating in the post-LS2 and post-LS3 scenarios. This is done to evaluate the impact on transverse beam stability of choosing uncoated

TABLE I. Collimator material scenarios investigated in simulations.

| Scenario | Primary collimators (TCP) | Secondary collimators (TCSG) |
|---|---|---|
| LHC 2017 | 3 CFC | 11 CFC |
| LHC 2017, TCSGs at $14\sigma_{\text{coll}}$ | 3 CFC | 11 CFC |
| HL-LHC post-LS2, uncoated TCSGs | 2 MoGr, 1 CFC | 4 MoGr, 7 CFC |
| HL-LHC post-LS2, coated TCSGs | 2 MoGr, 1 CFC | 4 Mo + MoGr, 7 CFC |
| HL-LHC post-LS3, uncoated TCSGs | 2 MoGr, 1 CFC | 11 MoGr |
| HL-LHC post-LS3, coated TCSGs | 2 MoGr, 1 CFC | 11 Mo + MoGr |

jaws. Uncoated jaws have the advantage of being easier to manufacture, at the expense of a larger electrical resistivity. Copper-coated graphite collimators are also being considered as an alternative to Mo-coated MoGr. However, this option is beyond the present operational scenario foreseen for HL-LHC [13].

The HL-LHC impedance model [31] was used to simulate the overall machine impedance for the post-LS2 and post-LS3 cases. It is developed from the LHC impedance model that accounts for the various elements shown in Fig. 2. The post-LS2 scenario accounts for the new collimation layout in IR7 only. The post-LS3 scenario accounts for the full collimation upgrade layout, which also includes changes to collimators outside of IR7. In the full impedance model, the collimator impedance accounts for the resistive wall impedance and the geometric impedance (respectively figured in light blue and dark blue in Fig. 2). Limits and validity of this approach have been addressed in [32], and the approach used for the LHC impedance model has been deemed sufficiently accurate. The calculation of the collimator resistive-wall impedance is performed using ImpedanceWake2D [33]. The code implements the field matching technique to compute the electromagnetic fields inside an infinitely long multilayered structure of circular or flat cross section [34]. The material resistivities used for the simulations are 5 μΩm for CFC, 1 μΩm for MoGr, and 0.053 μΩm for Mo [26].

The various scenarios considered for the study are summarized below and in Tables I and II. (i) First, the LHC impedance model with 2017 operational collimator settings is considered. All primary and secondary collimators are in CFC. (ii) A second LHC impedance model is studied, where the secondary collimators in IR7 are more open than the nominal operational settings, therefore decreasing the beam coupling impedance. (iii) The HL-LHC impedance model after LS2 with uncoated collimators. Two primary collimators (TCP) are replaced with MoGr, and four secondary collimators (TCSG) are replaced with MoGr. This scenario simulates a post-LS2 situation without coating on the TCSG, increasing the transverse impedance. (iv) The HL-LHC impedance model after LS2 with coated collimators. Two primary collimators (TCS) are replaced with MoGr, and four secondary collimators (TCSG) are replaced with Mo-coated MoGr. This scenario represents the baseline post-LS2 impedance. (v) The HL-LHC impedance model after LS3 with uncoated collimators. Two primary collimators (TCP) are replaced with MoGr, and eleven secondary collimators (TCSG) are replaced with MoGr. This scenario simulates the ultimate HL-LHC collimation upgrade without coating on the TCSGs, increasing the transverse impedance with respect to the next case. (vi) The HL-LHC impedance model after LS3 with coated collimators. Two primary collimators (TCP) are replaced with MoGr, and eleven secondary collimators (TCSG) are replaced with Mo-coated MoGr. This scenario represents the ultimate HL-LHC after the collimation upgrade.

TABLE II. Collimator settings in $N_{\sigma_{\text{coll}}}$ considered in the simulations.

| Scenario | TCP | TCSG |
|---|---|---|
| LHC 2017[a] | 5 | 6.5 |
| LHC 2017, TCSGs at 14 $\sigma_{\text{coll}}$[a] | 5 | 14 |
| HL-LHC post-LS2, uncoated TCSGs[b] | 6.7 | 7.9 |
| HL-LHC post-LS2, coated TCSGs[b] | 6.7 | 7.9 |
| HL-LHC post-LS3, uncoated TCSGs[b] | 6.7 | 7.9 |
| HL-LHC post-LS3, coated TCSGs[b] | 6.7 | 7.9 |

[a]Emittance $\varepsilon = 3.5$ μm rad.
[b]Emittance $\varepsilon = 2.5$ μm rad.

To compute the resistive-wall impedance contribution of each collimator, their physical half gap $h$ is needed. The transverse beam size at the collimator $\sigma_{\text{coll}}$ is given by

$$\sigma_{\text{coll}} = \sqrt{\beta_{x,y}\frac{\varepsilon_{x,y}}{\beta\gamma}} \tag{1}$$

with $\beta_{x,y}$ the Twiss beta functions, $\varepsilon_{x,y}$ the normalized transverse beam emittance, $\beta$ the particle speed in units of speed of light $c$, and $\gamma$ the relativistic Lorentz factor [35]. The beam size at the collimator does not include the dispersion term, and the emittance $\varepsilon_{x,y}$ was fixed to 3.5 μm rad for the LHC, whereas 2.5 μm rad is used for HL-LHC. Assuming the Twiss beta function remains the same at the collimator, the beam size $\sigma_{\text{HL-LHC}}$ in a HL-LHC collimator compared to the one in an LHC collimator $\sigma_{\text{LHC}}$ is therefore

$$\frac{\sigma_{\text{HL-LHC}}}{\sigma_{\text{LHC}}} = \sqrt{\frac{\varepsilon_{\text{HL-LHC}}}{\varepsilon_{\text{LHC}}}\frac{\gamma_{\text{LHC}}}{\gamma_{\text{HL-LHC}}}} = 0.81. \tag{2}$$

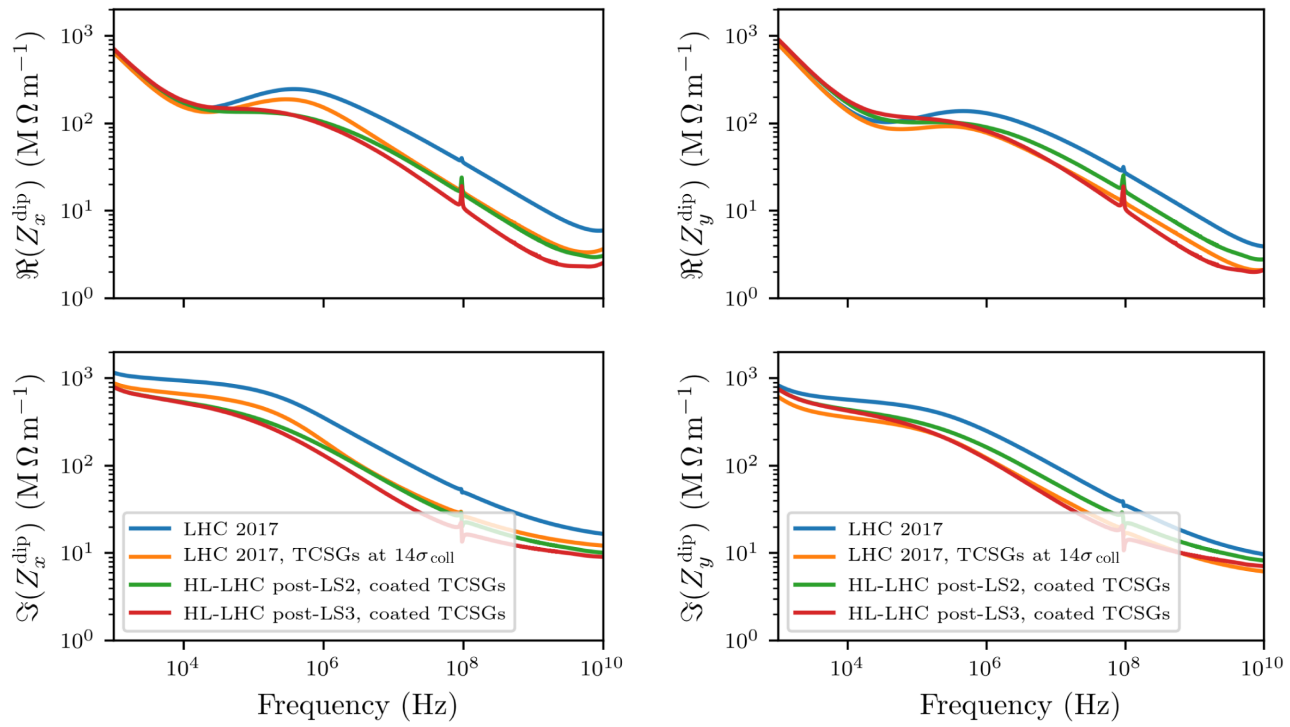


FIG. 4. Transverse dipolar beam coupling impedance of the full LHC for the considered scenarios of Tables I and II. For HL-LHC impedances, only the scenarios including coated collimators are reported. The impedance of the horizontal plane is shown in the left, and the one of the vertical plane in the right. The real and imaginary parts of the impedance are, respectively, shown at the top and bottom plots.

The physical half gap $h$ of each collimator in the LHC is often indicated with respect to the transverse beam size. This ratio $N_{\sigma_{\mathrm{coll}}}$ is given by

$$N_{\sigma_{\mathrm{coll}}} = h/\sigma_{\mathrm{coll}}. \tag{3}$$

The $N_{\sigma_{\mathrm{coll}}}$ in HL-LHC is different from LHC because of the smaller beam size and a change in the collimators configuration. This can be seen in Table II that reports the collimators gaps in $N_{\sigma_{\mathrm{coll}}}$ used for the simulations: the HL-LHC collimator parameters are set to a larger value than in LHC.

The horizontal and vertical total dipolar impedances as a function of frequency (both real and imaginary parts) are plotted in Fig. 4 for the different scenarios considered. All the simulated scenarios include the elements detailed in Fig. 2. A clear impedance reduction with respect to the LHC 2017 nominal case is predicted in the post-LS2 and post-LS3 simulations. The post-LS3 upgrade with all TCSGs made of Mo-coated MoGr provides a reduction by a factor ∼5 over the 10 kHz to 10 GHz frequency range with respect to the 2017 LHC operational impedance. The LHC scenario with the TCSGs opened at 14$\sigma_{\mathrm{coll}}$, represented in orange, is close to the post-LS2 scenario of the HL-LHC collimation upgrade, represented in green, in the 10 MHz to 10 GHz range and for the horizontal impedance. For the vertical impedance, in the same frequency range, the scenario with the TCSGs opened at 14$\sigma_{\mathrm{coll}}$ is close to the post-LS3 scenario (red curve).

The impedance models described beforehand for the LHC and HL-LHC upgrade are used to predict with simulation the tune shift versus intensity expected in the accelerator for the different collimator upgrade scenarios. The results of the tune shift simulations are presented in the next section.

### B. Simulation of the tune shift versus intensity for the different collimator scenarios

Beam stability simulations are performed with DELPHI [36,37], an analytic Vlasov solver, for the scenarios presented beforehand. DELPHI accounts for the dipolar impedance and the transverse damper to derive a linear system which is then diagonalized, and the eigenvalues are used to obtain the transverse growth rate and mode frequency shifts. The beam parameters used for the simulations are detailed in Table III.

Figure 5 shows DELPHI results obtained for the LHC 2017 scenario and the HL-LHC final scenario with Mo coating, at chromaticity $Q'_x = 0$. Only the single bunch, horizontal plane instability is reported since it is the most

TABLE III. Beam parameters used for the stability simulations at top energy.

| Parameter | LHC | HL-LHC |
|---|---|---|
| Machine | | |
| Circumference (m) | 26658.8832 | |
| Energy (TeV) | 6.5 | 7 |
| Transverse tunes $Q_x$, $Q_y$ | 62.31, 60.32 | |
| Momentum compaction factor $\alpha_c$ | $3.225 \times 10^{-4}$ | $3.455 \times 10^{-4}$ |
| rf voltage (MV) | 12 | 16 |
| Harmonic number | 35640 | |
| Synchrotron tune $Q_s$ | $1.838 \times 10^{-3}$ | $2.04 \times 10^{-3}$ |
| Beam | | |
| Number of bunches | 1 | |
| $4\sigma$ bunch length (ns) | 1.08 | |
| Bunch intensity ($1 \times 10^{11}$ p.p.b.) | 0 to 10 | |
| Chromaticity $Q'$ | 0 to 7 | |

critical from the stability point of view. This asymmetric behavior between the two planes comes from a difference between the vertical and horizontal impedances [13,28]. This plot shows that the beam azimuthal modes 0 and −1 are uncoupled below a certain intensity. As the bunch intensity increases, the mode frequencies approach each other, to a point where they couple. This point marks the intensity threshold of the TMCI. In the 2017 operational scenario, the TMCI threshold is predicted to occur at an intensity of $2.8 \times 10^{11}$ p.p.b. For the post-LS3 HL-LHC scenario, the threshold is increased to $8.4 \times 10^{11}$ p.p.b.

The TMCI intensity threshold can be inferred from the intersection of modes 0 and −1 shift versus intensity as shown in Fig. 5. Figure 6 shows, at the top, the mode 0 shift versus intensity for all the simulated scenarios from Table I, while at the bottom, the most unstable mode growth rate is shown. The onset of the TMCI occurs in correspondence to the intersection of mode 0 and −1.

The tune shifts versus intensity can be computed from the linear fit on the azimuthal mode 0 variation with intensity [38]. The values for each scenario are reported in Table IV. The first stage implementation of the collimation upgrade during the LS2 should increase the TMCI intensity threshold by a factor 2.2, from $2.8 \times 10^{11}$ to $6.3 \times 10^{11}$ p.p.b. The post-LS3 stage of the upgrade with 11 secondary collimators coated with Mo increases the TMCI threshold by a factor 3.1 compared to the 2017 LHC operational case. For all these scenarios, the TMCI threshold reaches a value higher than the maximum bunch intensity of $2.3 \times 10^{11}$ p.p.b. planned for HL-LHC.

Furthermore, the Mo coating used for the secondary collimators helps to increase the TMCI threshold by 10%

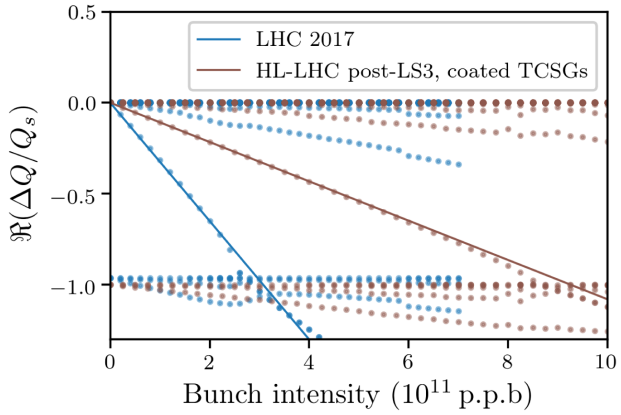


FIG. 5. Horizontal mode frequency shifts as a function of bunch intensity for the LHC 2017 operational scenario and the post-LS3 HL-LHC scenario. The modes (points) are computed with DELPHI and the mode 0 is then fitted in solid lines in the low intensity range (i.e., between 0 and $1 \times 10^{11}$ p.p.b.) and the plot is extrapolated to higher intensities.

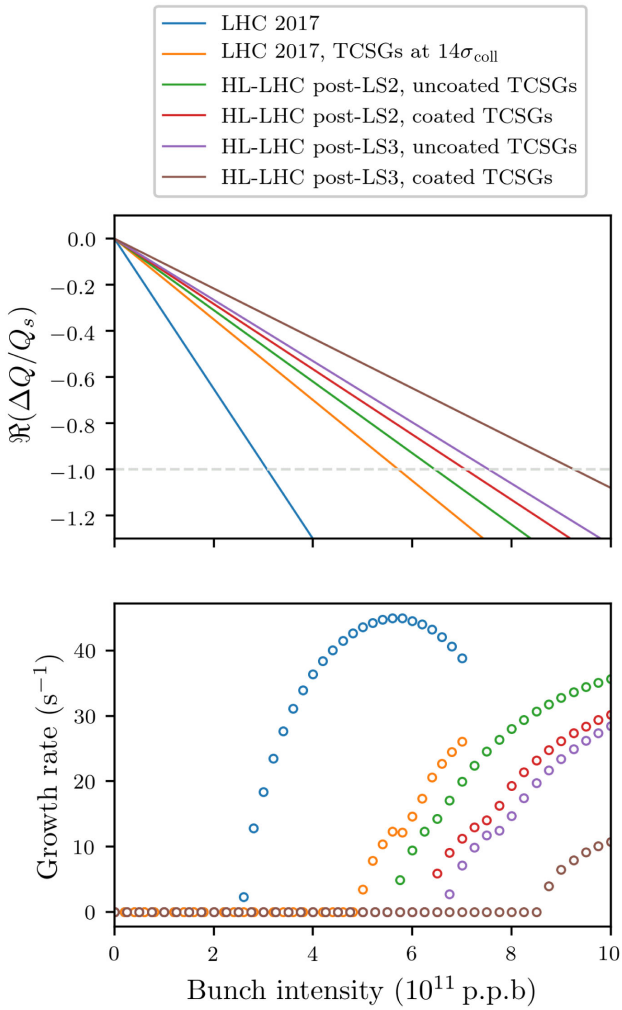


FIG. 6. Tune shift (upper plot) and most unstable mode growth rate (lower plot) as a function of bunch intensity for the different impedance scenarios considered. In the upper plot, the tune shift slope has been calculated in the intensity range from 0 to $1 \times 10^{11}$ p.p.b. range.

TABLE IV. Results of DELPHI simulations for the LHC and HL-LHC impedance reduction scenarios. Both the tune shift versus intensity and the TMCI threshold are reported.

| Scenario | Tune shift $[(10^{11}\ \text{p.p.b.} \times Q_s)^{-1}]$ | TMCI threshold ($10^{11}$ p.p.b.) |
|---|---|---|
| LHC 2017 operational setting | −0.32 | 2.8 |
| LHC 2017, TCSGs at $14\sigma_{\text{coll}}$ | −0.18 | 5.0 |
| HL-LHC post-LS2, uncoated TCSGs | −0.16 | 5.7 |
| HL-LHC post-LS2, coated TCSGs | −0.14 | 6.3 |
| HL-LHC post-LS3, uncoated TCSGs | −0.13 | 6.7 |
| HL-LHC post-LS3, coated TCSGs | −0.11 | 8.7 |

for the LS2 upgrade and by 30% for the final upgrade with respect to uncoated collimators. Still, a large intensity margin for the TMCI threshold is present in case of accidental coating degradation on the secondary collimators.

The 2017 LHC scenario with TCSG gaps at $14\sigma_{\text{coll}}$ is predicted to be close to the post-LS2 uncoated scenario. This scenario is used for beam-based measurements in the LHC presented in Sec. III.

Operational experience in the LHC showed that the transverse damper and a positive chromaticity are required to prevent coherent beam instabilities. The effect of a positive chromaticity of $Q' = 5$ was also simulated for both horizontal and vertical planes. Simultaneously, a transverse damping time corresponding to 100 turns was also included. This setting corresponds to a standard run 2 configuration. Figure 7 compares the tune shift and growth rate for the LHC 2017 scenario, without and with chromaticity and transverse damping. When chromaticity and damper are included, the tune shift as a function of intensity remains approximately the same with respect to the one corresponding to $Q' = 0$ and the absence of transverse damper, as long as the intensity remains below $2 \times 10^{11}$ p.p.b. However, the fast instability is suppressed at all intensities. This will allow to estimate the TMCI threshold through measurements in the LHC while keeping the beam stable with a transverse damper and a positive chromaticity.

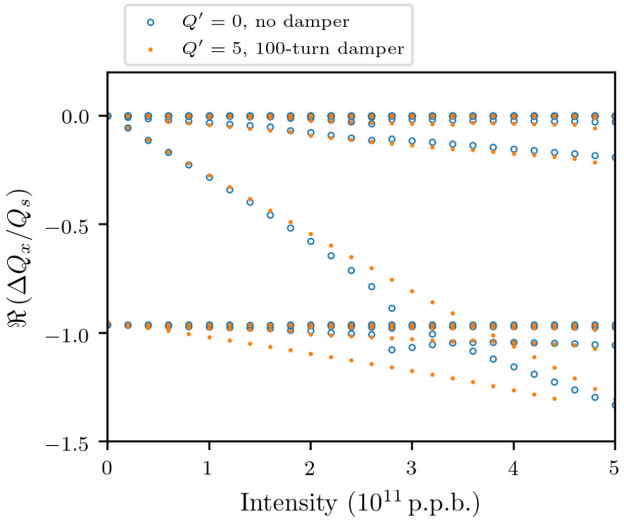


FIG. 7. Comparison of the mode frequency shift for $Q' = 0$ and no damper (blue dots) and for $Q' = 5$ and a 100-turn damping time (orange dots). The impedance scenario is the LHC 2017 operational one.

## III. TMCI MEASUREMENTS IN THE LHC

The tune shift simulations presented in the previous section were used to guide the measurement procedure performed afterward in the LHC. In Sec. III A, we will detail the machine and measurement setup. The results of the tune shift measurement and the inferred TMCI thresholds are then detailed in Sec. III B. Additional simulations of the impedance model and the induced tune shift are also performed after the measurement, using the collimator half-gaps that were actually in the machine. Simulations and measurements could then be compared more precisely.

### A. Machine configuration and measurement setup

Following the simulation results presented in Sec. II, the TMCI threshold in the LHC was measured by tracking the tune of bunches with different intensities and extrapolating the crossing point with the mode −1. A dedicated measurement was performed in the LHC in September 2017 [39]. As shown by the difference between the LHC 2017 operational scenario and the LHC scenario with TCSGs at $14\sigma_{\text{coll}}$ (presented in Fig. 4), the LHC transverse impedance can be significantly changed by moving the collimator gaps. However, opening the collimators reduces the halo cleaning efficiency and therefore increases the risk of provoking a magnet quench. Because of the machine protection requirements, the secondary collimators can have their gaps opened to $14\sigma_{\text{coll}}$ only if the total intensity in each beam is kept below $3 \times 10^{11}$ protons. To obtain enough points in the bunch intensity range, measurements were therefore split between two LHC energy ramps. A first energy ramp was done during LHC fill number 6210 where three bunches with $0.6 \times 10^{11}$, $1 \times 10^{11}$, and $1.2 \times 10^{11}$ p.p.b. were brought to the top energy of 6.5 TeV. A second energy ramp was performed during fill 6212 where two bunches with $0.8 \times 10^{11}$ and $1.9 \times 10^{11}$ p.p.b. were used.

TABLE V. IR7 collimator settings in $N_{\sigma_{\text{coll}}}$ used for the tune shift measurement (with a reference emittance of 3.5 μm). Scenario 1 corresponds to relaxed settings reproducing the expected post-LS2 impedance. Scenario 2 is the operational collimator setting in 2017. Scenarios 3 and 4 are tighter settings used to increase the overall machine impedance. The last column indicates in which fill the scenarios were used.

| Scenario | Scenario number | TCP setting | TCSG setting | Fill |
|---|---|---|---|---|
| LHC 2017, TCSGs at $14\sigma_{\text{coll}}$ | 1 | 5 | 14 | 6212 |
| LHC 2017 | 2 | 5 | 6.5 | 6210 and 6212 |
| LHC 2017, tighter TCSG | 3 | 5 | 6 | 6210 and 6212 |
| LHC 2017, tighter TCP and TCSG | 4 | 4.5 | 6 | 6210 and 6212 |

At top energy, the chromaticity was reduced from $Q' \sim 15$ to $Q' \sim 4$ for both planes of beams 1 and 2, so that the tune shift would not be too much affected by chromaticity, as illustrated in Fig. 7. Primary and secondary collimators settings in IR7 were then modified to increase or decrease the machine impedance. Table V reports the different settings in $N_{\sigma_{\text{coll}}}$ which were measured during the two energy ramps.

The LHC transverse damper was used as a controlled source of excitation and the oscillation signal of individual bunches was recorded using the damper stripline pickups [40,41]. This method was developed for collimator impedance measurement [42–45]: it provides flexible control of the excitation strength and allows to select specific bunches to excite.

The turn-by-turn oscillation signal of each bunch is recorded over 8000 turns with the ADT-ObsBox [41], the electronic unit processing raw data from the transverse damper stripline pickups. From these oscillation signals, the tune of each bunch is reconstructed using PySUSSIX [46], a Python wrapper of the SUSSIX code [47], which performs an iterative frequency analysis of the time domain data to extract the fundamental and harmonic frequencies present in the signal. The transverse kick amplitude was set to provide an oscillation over at least 500 turns before transverse decoherence.

### B. Analysis of measurement results and comparison with simulations predictions

Measurement results were compared to DELPHI simulations using the LHC beam parameters presented in Table III. For each scenario in Table V, the machine impedance model was recomputed using the physical collimator gap measured from the collimators motor positions, retrieved from the LHC logging database [48]. The effect of quadrupolar impedance on the tune shift was also accounted for [38]: for each scenario, Sacherer's formula [49] is used to compute the tune shift induced by the dipolar and quadrupolar impedances separately, respectively, $\Delta Q_{\text{dip}}$ and $\Delta Q_{\text{quad}}$. A correction factor to account for the quadrupolar impedance is defined as $(\Delta Q_{\text{dip}} + \Delta Q_{\text{quad}})/\Delta Q_{\text{dip}}$, which is then applied to the tune shift versus intensity computed with DELPHI (which accounts for the dipolar impedance only). This method allows for an analytical estimation of the quadrupolar impedance effect and the results it yields are compatible with the precision typically obtained with tune shift measurements. Self-consistent simulation of the effect of detuning impedance on the tune shift is nevertheless planned using eDELPHI and PyHEADTAIL [50]. Measurement and simulation results are reported in Figs. 8 and 9, which show the measured tune shifts for the 2017 operational settings (scenario 2) and tighter settings (scenarios 3 and 4). Crosses represent measurements taken during the first fill, dots measurements taken during the second fill, and dashed lines DELPHI simulations.

Figures 8 and 9 clearly show the effect of the impedance reduction (or increase) on the tune shift versus intensity, depending on the relaxed (or tighter) collimator settings. For example, with scenario 2 reproducing an equivalent post-LS2 impedance (red line and dots) a clear tune shift reduction is obtained with respect to the 2017 LHC operational scenario (blue line and dots).

The tune shifts deduced from the measurement are reported in Table VI. The slope, accounting for the uncertainty, was obtained by performing a linear fit on the data points shown in Figs. 8 and 9. To be able to merge the data from the two fills, the zero intensity tune value fitted for each fill was subtracted from the data points. Overall, Figs. 8 and 9 show that tune shifts simulated with the impedance model are in reasonable agreement with measurements. However, tune shift slope variations can be observed, which is related to the reproducibility of the machine between the two different fills.

The approximate TMCI threshold can be extrapolated from the tune shift measurement, as detailed in Sec. II. Results in Table VI show that with relaxed collimators settings, the tune shift is decreased, and the TMCI threshold is increased. This supports the benefit of the global impedance reduction planned for HL-LHC during LS2 and LS3 with a global measurement.

The measurement with tighter collimator gaps than the LHC 2017 operational scenario also allowed to compare the impedance model to measurements. Table VI also reports the tune shifts predicted with DELPHI simulations, which are derived from the LHC impedance model and use the actual collimator gaps.

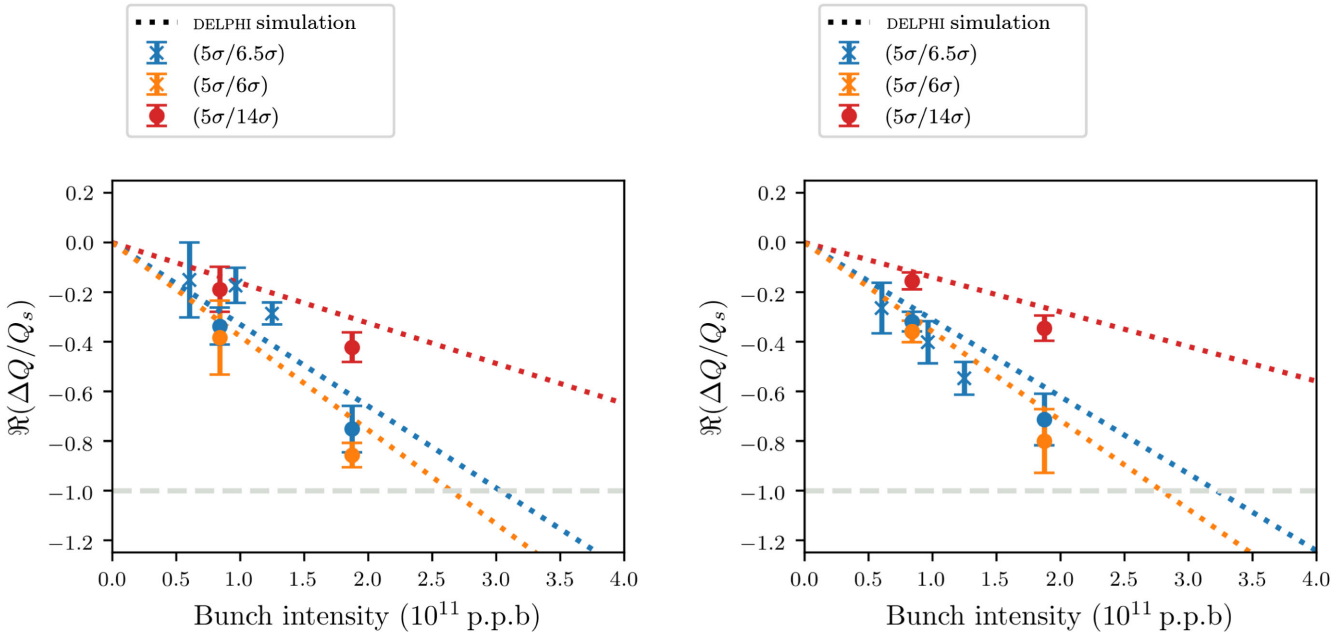


FIG. 8. Measurement of the beam 1 tune shift versus intensity for different sets of collimator settings compared to DELPHI simulations (dotted lines). Error bars represent the standard deviation of all tune measurements recorded for each bunch intensity and collimator configuration. Fill 6210 data are represented with crosses and fill 6212 data with circles. On the left and right plots, the horizontal and vertical planes are, respectively, shown.

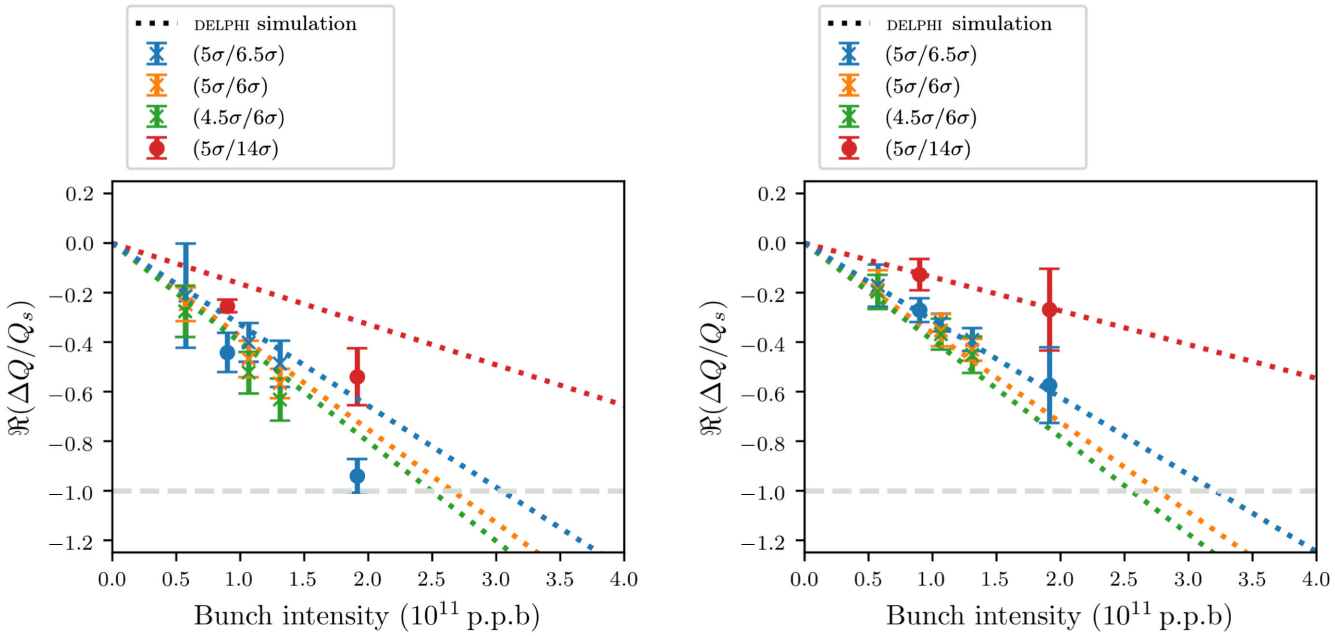


FIG. 9. Measurement of the beam 2 tune shift versus intensity for different sets of collimator settings compared to DELPHI simulations (dotted lines). Error bars represent the standard deviation of all tune measurements recorded for each bunch intensity and collimator configuration. Fill 6210 data are represented with crosses and fill 6212 data with circles. On the left and right plots, the horizontal and vertical planes are, respectively, shown.

TABLE VI. Measured and simulated tune shifts for the LHC relaxed, 2017 operational and tighter collimator settings. The "Scenario" column gives the scenario from Table V and the corresponding TCP/TCSG setting in $\sigma_{\text{coll}}$. The following columns report the tune shift slope values normalized to the synchrotron tune $Q_s = 1.9 \times 10^{-3}$ and a bunch intensity of $1 \times 10^{12}$ p.p.b. computed with DELPHI ("Sim."), the correction factor to account for the quadrupolar impedance effect ("Corr. factor") and the tune shift accounting for the correction factor ("Sim. w/quad."). The "Measured" column is the measurement result obtained by linear fitting the tune variation measured at different intensities, with the corresponding errorbar. The "Ratio" column computes the ratio between tune shift from simulation (with quadrupolar impedance) and the average measured one.

| | | | Tune shift ($10^{-12}$ p.p.b. $\times Q_s$) | | | | |
|---|---|---|---|---|---|---|---|
| Fill | Plane | Scenario number | Sim. | Corr. factor | Sim. w/quad. | Measured | Ratio |
| 6210 | B1H | 2 (5/6.5) | −4.1 | 0.81 | −3.3 | −2.2(3) | 1.50 |
| | B1V | 2 (5/6.5) | −3.4 | 0.92 | −3.1 | −4.3(4) | 0.72 |
| | B2H | 2 (5/6.5) | −4.0 | 0.82 | −3.3 | −3.8(5) | 0.86 |
| | | 3 (5/6.0) | −4.7 | 0.81 | −3.9 | −4.4(4) | 0.89 |
| | | 4 (4.5/6.0) | −5.0 | 0.81 | −4.0 | −4.9(5) | 0.81 |
| | B2V | 2 (5/6.5) | −3.4 | 0.92 | −3.1 | −3.0(2) | 1.03 |
| | | 3 (5/6.0) | −3.9 | 0.93 | −3.6 | −3.3(3) | 1.09 |
| | | 4 (4.5/6.0) | −4.2 | 0.93 | −3.9 | −3.5(4) | 1.11 |
| 6212 | B1H | 1 (5/14) | −1.9 | 0.86 | −1.6 | −2.3(3) | 0.70 |
| | | 2 (5/6.5) | −4.1 | 0.81 | −3.3 | −4.0(4) | 0.82 |
| | | 3 (5/6.0) | −4.7 | 0.81 | −3.8 | −4.6(3) | 0.83 |
| | B1V | 1 (5/14) | −1.6 | 0.85 | −1.4 | −1.8(2) | 0.77 |
| | | 2 (5/6.5) | −3.4 | 0.92 | −3.1 | −3.8(4) | 0.82 |
| | | 3 (5/6.0) | −3.9 | 0.92 | −3.6 | −4.3(4) | 0.83 |
| | B2H | 1 (5/14) | −1.9 | 0.86 | −1.6 | −2.8(3) | 0.57 |
| | | 2 (5/6.5) | −4.0 | 0.82 | −3.3 | −4.9(3) | 0.67 |
| | B2V | 1 (5/14) | −1.6 | 0.85 | −1.4 | −1.4(5) | 1.0 |
| | | 2 (5/6.5) | −3.4 | 0.92 | −3.1 | −3.0(4) | 1.03 |

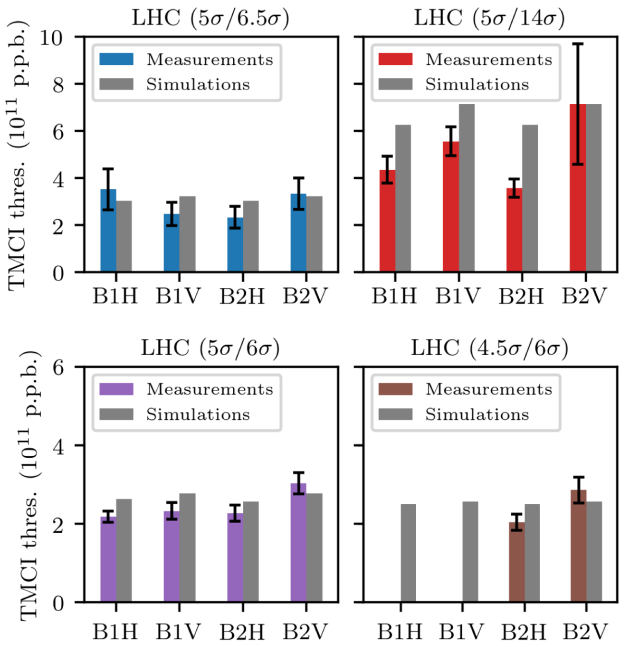


FIG. 10. Comparison of the TMCI threshold extrapolated from measurement (color bars) versus DELPHI simulation (gray bars) for the different LHC collimation scenarios: scenarios 2, 1, 3, and 4 from left to right and top to bottom.

As expected and predicted with simulations, tighter collimator gaps lead to an increased tune shift versus intensity. The measurement also allowed to estimate the discrepancy between the impedance model and the real machine impedance through the TMCI threshold estimation. Figure 10 reports the extrapolated and simulated TMCI threshold from Table VI. After averaging over the four measurements with different collimator gaps, the model appears to overestimate the TMCI threshold (e.g., underestimate the tune shift) by 20% except for the vertical plane of Beam 2 where it seems to underestimate it by 10%. Tune shifts measured with the $(5\sigma/14\sigma)$ collimator gaps are smaller and therefore the tune shift slope decreases. In turn, the relative errors become larger as well as the discrepancies with respect to the model. The discrepancy could also originate from the assumptions used for tune shift simulations or from other sources of impedance not accounted for in the model. Additional measurements, such as impedance localization are foreseen in the LHC [51,52].

## IV. CONCLUSIONS

In this study, we presented a detailed analysis of the transverse mode coupling instability in the LHC, with a

particular focus on the impact of the collimation system on the machine beam coupling impedance, and the effect on the TMCI threshold. The importance of the impedance reduction planned in the HL-LHC framework has been highlighted through simulations, showing a potential increase of the TMCI threshold by a factor 3 compared to the 2017 LHC operational configuration.

Dedicated measurements in the LHC confirmed the benefits of the impedance reduction. The tune shift as a function of intensity was measured at the LHC top energy. The measurement was carried out for multiple collimator configurations, taking advantage of these movable devices to act as a tunable source of beam coupling impedance. The beneficial effect of the impedance reduction was further confirmed with a collimator configuration mimicking an equivalent HL-LHC impedance. Probing multiple configurations also highlighted a 20% overestimate of the TMCI threshold by the LHC impedance model except for the vertical plane of beam 2 where the threshold is underestimated by 10%.

As new low-impedance collimators were installed during long shutdown 2, further beam-based measurements were performed at the start of the new LHC run and are currently being analyzed. Further investigations of the geometric impedance of the collimators also helped to improve the design of the tapering sections, in the framework of the LHC and HL-LHC impedance reduction.

## ACKNOWLEDGMENTS

This work has been supported by the HL-LHC project. The authors would also like to acknowledge the LHC and Injectors operation and coordination teams for their support in the preparation and the execution of the beam measurements. They also thank the LHC collimation working group for the input and remarks regarding the collimation upgrade project.

[1] N. Wang, Y. Zhang, Y. Liu, S. Tian, K. Ohmi, and C. Lin, Mitigation of coherent beam instabilities in CEPC, in *Proceedings of the ICFA Mini-Workshop on Mitigation of Coherent Beam Instabilities in Particle Accelerators, Zermatt, Switzerland* (CERN, Geneva, Switzerland, 2020).

[2] M. Zobov, E. Belli, R. Kersevan, A. Novokhatski, S. Zadeh, and M. Migliorati, Mitigation of the impedance-related collective effects in FCC-ee, in *Proceedings of the ICFA Mini-Workshop on Mitigation of Coherent Beam Instabilities in Particle Accelerators, Zermatt, Switzerland* (CERN, Geneva, Switzerland, 2020).

[3] R. Williamson, B. Jones, A. Pertica, D. Posthuma de Boer, C. Warsop, and J. Komppula, Measurements and damping of the ISIS head-tail instability, in *Proceedings of the ICFA Mini-Workshop on Mitigation of Coherent Beam Instabilities in Particle Accelerators, Zermatt, Switzerland* (CERN, Geneva, Switzerland, 2020).

[4] Y. Chin, Analysis of transverse instabilities observed at J-PARC MR and their suppression using feedback systems, in *Proceedings of the 25th Particle Accelerator Conference, PAC-2013, Pasadena, CA, 2013* (JACoW, CERN, Geneva, Switzerland, 2013), pp. 27–31.

[5] M. Migliorati, E. Métral, and M. Zobov, Review of impedance-induced instabilities and their possible mitigation techniques, in *Proceedings of the ICFA Mini-Workshop on Mitigation of Coherent Beam Instabilities in Particle Accelerators, Zermatt, Switzerland* (CERN, Geneva, Switzerland, 2020).

[6] E. Métral *et al.*, Measurement and interpretation of transverse beam instabilities in the CERN Large Hadron Collider (LHC) and extrapolations to HL-LHC, in *Proceedings of ICFA Advanced Beam Dynamics Workshop on High-Intensity and High-Brightness Hadron Beams (HB'16), Malmö, Sweden, 2016* (JACoW, CERN, Geneva, Switzerland, 2016), pp. 254–259.

[7] B. Salvant *et al.*, LHC impedance model: Experience with high intensity operation in the LHC, in *Proceedings of ICFA Advanced Beam Dynamics Workshop on High-Intensity and High-Brightness Hadron Beams (HB'12), Beijing, China, 2012* (JACoW, CERN, Geneva, Switzerland, 2013).

[8] L. R. Carver, X. Buffat, K. Li, E. Métral, and M. Schenk, Transverse beam instabilities in the presence of linear coupling in the Large Hadron Collider, Phys. Rev. Accel. Beams **21**, 044401 (2018).

[9] X. Buffat *et al.*, Transverse instabilities, in *Proceedings of the 9th LHC Operations Evian Workshop, Evian Les Bains, France* (CERN, Geneva, Switzerland, 2019).

[10] S. A. Antipov, D. Amorim, N. Biancacci, X. Buffat, E. Métral, N. Mounet, A. Oeftiger, and D. Valuch, Proof-of-principle direct measurement of Landau damping strength at the large hadron collider with an antidamper, Phys. Rev. Lett. **126**, 164801 (2021).

[11] L. R. Carver, N. Biancacci, E. Métral, B. Salvant, T. Levens, X. Buffat, T. Pieloni, C. Tambasco, and G. Trad, MD 346—Summary of single bunch instability threshold measurements, CERN, LHC MD Note No. CERN-ACC-NOTE-2016-0002, 2016.

[12] I. Béjar Alonso *et al.*, High-Luminosity Large Hadron Collider (HL-LHC): Technical design report, CERN, CERN Yellow Reports: Monographs CERN-2020-010, 2020.

[13] E. Métral *et al.*, Update of the HL-LHC operational senarios for proton operation, CERN Technical Report No. CERN-ACC-NOTE-2018-0002, 2018.

[14] B. Salvachua, Overview of proton-proton physics during run 2, in *Proceedings of the 9th LHC Operations Evian Workshop, Evian Les Bains, France* (CERN, Geneva, Switzerland, 2019).

[15] R. Nagaoka, Design optimization and impedance sources in Low Emittance Rings (LERs), in *Proceedings of the ICFA Mini-Workshop on Mitigation of Coherent Beam Instabilities in Particle Accelerators, Zermatt, Switzerland* (CERN, Geneva, Switzerland, 2020).

[16] D. Schulte, Mitigation of coherent beam instabilities in linear colliders and FCC-hh, in *Proceedings of the ICFA*

*Mini-Workshop on Mitigation of Coherent Beam Instabilities in Particle Accelerators, Zermatt, Switzerland* (CERN, Geneva, Switzerland, 2020).

[17] R. Assmann *et al.*, The final collimation system for the LHC, in *Proceedings of 10th European Particle Accelerator Conference, Edinburgh, Scotland, 2006* (EPS-AG, Edinburgh, Scotland, 2006).

[18] R. Bruce *et al.*, Simulations and measurements of beam loss patterns at the CERN Large Hadron Collider, Phys. Rev. ST Accel. Beams **17**, 081004 (2014).

[19] M. Church, A. I. Drozhdin, L. A., N. V. Mokhov, and R. Reilly, Tevatron run-II beam collimation system, in *Proceedings of the 18th Particle Accelerator Conference, New York* (IEEE, New York, 1999), pp. 56–58.

[20] T. Ishibashi, S. Terui, Y. Suetsugu, K. Watanabe, and M. Shirai, Movable collimator system for SuperKEKB, Phys. Rev. Accel. Beams **23**, 053501 (2020).

[21] Y. Jiao *et al.*, Progress of lattice design and physics studies on the high energy photon source, in *Proceedings of the 10th International Particle Accelerator Conference (IPAC'19), Melbourne, Australia, 2019* (2019), pp. 1510–1513, 10.18429/JACoW-IPAC2019-TUPGW046.

[22] A. Xiao and M. Borland, Beam loss simulation and collimator system configurations for the advanced photon source upgrade, in *Proceedings of North American Particle Accelerator Conference, 2016, Chicago, IL, USA* (JACoW, Geneva, Switzerland, 2017).

[23] J. Borrel, Y. Dabin, F. Ewald, and P. Van Vaerenbergh, Collimator for ESRF-EBS, in *Proceedings of the 10th Mechanical Engineering Design of Synchrotron Radiation Equipment and Instrumentation (MEDSI'18), Paris, France, 2018* (JACoW, Geneva, Switzerland, 2018), pp. 23–25, 10.18429/JACoW-MEDSI2018-TUPH02.

[24] J. Guardia-Valenzuela, A. Bertarelli, F. Carra, N. Mariani, S. Bizzaro, and R. Arenal, Development and properties of high thermal conductivity molybdenum carbide-graphite composites, Carbon **135**, 72 (2018).

[25] F. Carra, A. Bertarelli, G. Gobbi, J. Guardia-Valenzuela, M. Guinchard, F. Harden, M. Pasquali, S. Redaelli, and E. Skordis, Mechanical robustness of HL-LHC collimator designs, J. Phys. Conf. Ser. **1350**, 012083 (2019).

[26] C. Accettura *et al.*, Resistivity characterization of molybdenum-coated graphite-based substrates for high-luminosity LHC collimators, Coatings **10**, 361 (2020).

[27] S. A. Antipov *et al.*, Transverse beam stability with low-impedance collimators in the High-Luminosity Large Hadron Collider: Status and challenges, Phys. Rev. Accel. Beams **23**, 034403 (2020).

[28] S. Redaelli *et al.*, Staged implementation of low-impedance collimation in IR7: Plans for LS2, CERN Technical Report No. CERN-ACC-NOTE-2019-0001, 2019.

[29] S. Redaelli, R. Bruce, A. Lechner, and A. Mereghetti, Chapter 5: Collimation system, CERN Yellow Rep. Monogr. **10**, 87 (2020).

[30] E. Métral, Impedance models, operational experience and expected limitations (2019), in *Proceedings of the International Review of the HL-LHC Collimation System* (CERN, Geneva, Switzerland, 2019).

[31] D. Amorim *et al.*, HL-LHC impedance and related effects, CERN Technical Report No. CERN-ACC-NOTE-2018-0087, 2018.

[32] N. Biancacci *et al.*, 2D and 3D collimator impedance modelling and experimental results, in *Proceedings of ICFA Mini-Workshop on Impedances and Beam Instabilities in Particle Accelerators, Benevento, Italy* (CERN, Geneva, Switzerland, 2018).

[33] N. Mounet, ImpedanceWake2D, https://twiki.cern.ch/twiki/bin/view/ABPComputing/ImpedanceWake2D (2012), accessed on March 15, 2021.

[34] N. Mounet, The LHC transverse coupled-bunch instability, Ph.D. thesis, École Polytechnique Fédérale de Lausanne, 2012.

[35] S. Redaelli, Beam cleaning and collimation systems, in *Proceedings of the Joint International Accelerator School on Beam Loss and Accelerator Protection, Newport Beach, CA* (CERN, Geneva, Switzerland, 2016).

[36] N. Mounet, DELPHI: An analytic Vlasov Solver for impedance-driven modes, CERN Technical Report No. CERN-ACC-SLIDES-2014-0066, 2014.

[37] N. Mounet, Direct Vlasov solvers, arXiv:2006.09080.

[38] D. Amorim, Study of the transverse mode coupling instability in the CERN Large Hadron Collider, Ph.D. thesis, Université Grenoble-Alpes, 2019.

[39] D. Amorim *et al.*, MD2490—Measurement of the TMCI threshold at flat-top in the LHC, CERN, LHC MD Note No. CERN-ACC-NOTE-2020-0056, 2020.

[40] D. Valuch, Excitation by ADT and active bunch by bunch tune measurements, in *Proceedings of the 129th SPS and LHC Machine Protection Panel Meeting* (CERN, Geneva, Switzerland, 2016).

[41] M. Soderen and D. Valuch, ADT ObsBox data acquisition, The LHC Beam Operation Committee (CERN, Geneva, Switzerland, 2017).

[42] A. Mereghetti *et al.*, MD1447-$\beta^*$—Reach: 2016 IR7 collimation hierarchy limit and impedance, CERN, LHC MD Note No. CERN-ACC-NOTE-2020-0021, 2020.

[43] A. Mereghetti *et al.*, MD1446-$\beta^*$—Reach: Impedance contribution of primary collimators, CERN, LHC MD Note No. CERN-ACC-NOTE-2020-0020, 2020.

[44] A. Mereghetti *et al.*, MD2193—Impedance measurements of the TCSPM prototype collimator, CERN, LHC MD Note No. CERN-ACC-NOTE-2021-0021, 2021.

[45] A. Mereghetti *et al.*, MD1875—Impedance contribution of single IR7 secondary collimators, CERN, LHC MD Note No. CERN-ACC-NOTE-2020-0022, 2020.

[46] K. Li and R. Bartolini, CERN, and XBologna University, PySUSSIX, https://github.com/PyCOMPLETE/PySUSSIX (2013), accessed on March 15, 2021.

[47] R. Bartolini and F. Schmidt, A computer code for frequency analysis of non-linear betatron motion, CERN Technical Report No. SL-Note-98-017-AP, 1998.

[48] R. De Maria *et al.*, PyTimber, Python wrapping of the CERN Accelerator Logging Service (CALS) API., https://gitlab.cern.ch/scripting-tools/pytimber/ (2021), accessed on March 15, 2021.

[49] F. Sacherer, Transverse—Part II: Bunched beams, in *Proceedings of the 1st International School of Particle Accelerators "Ettore Majorana"* (CERN, Geneva, Switzerland, 1977).

[50] G. Iadarola, L. Mether, N. Mounet, and L. Sabato, Linearized method for the study of transverse instabilities driven by electron clouds, Phys. Rev. Accel. Beams **23**, 081002 (2020).

[51] N. Biancacci *et al.*, Impedance localization and identification, in *Proceedings of ICFA Mini-Workshop on Mitigation of Coherent Beam Instabilities in Particle Accelerators (MCBI 2019), Zermatt, Switzerland, 2019* (CERN, Geneva, Switzerland, 2020).

[52] N. Biancacci and R. Tomás, Using ac dipoles to localize sources of beam coupling impedance, Phys. Rev. Accel. Beams **19**, 054001 (2016).